Nonlinear wave propagation in free-electron lasers

R. Graham and S. Isermann
Fachbereich Physik, Universität Gesamthochschule Essen, D4300 Essen, Germany
(Received 25 September 1990)

The nonlinear coupled wave equations of a free-electron laser in the Compton regime are analyzed numerically and analytically, taking into account the shot noise in the incident electron beam. The influence of the sideband instability and the shot noise on the emitted spectrum are determined.

I. INTRODUCTION

A free-electron laser (FEL) consists of a collimated bunch of highly relativistic electrons passing a transversal magnetic field periodically modulated in the direction of propagation ("undulator"). The electrons are periodically accelerated transversal to their direction of propagation and hence radiate in the forward direction, providing the necessary gain.

A closed set of nonlinear partial differential equations describing this effect can be derived (cf., e.g., Refs. 1 and 2). One first considers the electron's motion in the combined electromagnetic field of the undulator and the radiation field. This motion generates the transversal current acting as a source term in Maxwell's equations and in turn produces the radiation field. Longitudinal current effects are negligible in electron beams of a density sufficiently low ($n_0 < 10^{13}$ cm^{-3}) to avoid the appearance of plasma oscillations. The equations obtained take the form[1,2]

$$\left[\frac{\partial}{\partial z}+\frac{1}{c}\frac{\partial}{\partial t}\right]E=-2\pi iK\frac{n_e}{\Sigma}\frac{1}{N}\sum_j\frac{1}{\gamma_j}e^{-i\sigma_j}\ , \tag{1.1}$$

$$\frac{d\sigma_i}{dt}=\frac{2\pi c}{\lambda_0}\left[1-\frac{\gamma_r^2}{\gamma_i^2}\right]\ , \tag{1.2}$$

$$\frac{d\gamma_i}{dt}=-\frac{ieK}{2\gamma_i m_0}(Ee^{i\sigma_i}-\text{c.c.})\ . \tag{1.3}$$

Here we assumed that a helical magnetic field

$$\mathbf{B}_0=\frac{B_0}{\sqrt{2}}(\mathbf{e}e^{-ik_0z}+\text{c.c.})\ , \tag{1.4}$$

with parameters

$$\mathbf{e}=(\mathbf{e}_x+i\mathbf{e}_y)/\sqrt{2},\quad \lambda_0=2\pi/k_0,\quad K=\frac{eB_0}{k_0m_0c^2}\ ,$$

is generated by the undulator. $E(z,t)$ is the slowly varying amplitude of the circularly polarized radiation field

$$\mathbf{E}=\frac{-i}{\sqrt{2}}(\mathbf{e}Ee^{ik(z-ct)}-\text{c.c.})\ ,$$

$$\mathbf{B}=\mathbf{e}_z\times\mathbf{E}\ , \tag{1.5}$$

$$\lambda=\frac{2\pi}{k},\quad \gamma_r^2=\frac{\lambda_0}{2\lambda}(1+K^2)\ .$$

The charge per unit length along the electron beam is n_e. It is assumed to be constant within the beam. The energy of the ith electron is $\gamma_i=m_i/m_0$ where m is its relativistic mass and m_0 its rest mass. The "phase" σ_i of the ith electron relative to the electromagnetic field is defined as

$$\sigma_i=(k_0+k)z_i-ckt\ . \tag{1.6}$$

Σ is the cross section of overlap between the electron beam and the undulator field. The sum in Eq. (1.1) is taken over all $N=n_e\lambda/e$ electrons within an optical wavelength λ centered around z at time t.

With the help of the "Pierce parameter"

$$\rho=\frac{1}{\gamma_r}\left[\frac{K\omega_p}{4\omega_0}\right]^{2/3},\qquad \omega_p=\left[\frac{4\pi e^2n_0}{m_0}\right]^{1/2}, \tag{1.7}$$

where n_0 is the number density of electrons, and assuming $\rho\ll1$ ($\rho\simeq2\times10^{-3}$ for the Stanford FEL), $(\gamma_i-\gamma_r)/\gamma_r\ll1$, the coupled wave equations may be put into the dimensionless and parameter-free form

$$\frac{\partial\sigma_i(\eta,\tau)}{\partial\tau}=p_i(\eta,\tau)\ , \tag{1.8}$$

$$\frac{\partial p_i(\eta,\tau)}{\partial\tau}=-[A(\eta,\tau)e^{i\sigma_i(\eta,\tau)}+\text{c.c.}]\ , \tag{1.9}$$

$$\left[\frac{\partial}{\partial\tau}+v\frac{\partial}{\partial\eta}\right]A(\eta,\tau)=\frac{1}{N}\sum_{i=1}^{N}e^{-i\sigma_i(\eta,\tau)}\ , \tag{1.10}$$

with

$$\tau=2\rho ck_0t\ ,\qquad \eta=2\rho k_0(z-\beta_\parallel ct)\ ,\qquad v=1-\beta_\parallel\ , \tag{1.11}$$

where $\beta_\parallel=v_\parallel/c$ is the dimensionless mean velocity of the electrons in the z direction,

$$\rho p_i=\frac{\gamma_i-\gamma_r}{\gamma_r}\ ,\qquad |A|^2=(\lambda\Sigma/4\pi\rho N\gamma_r mc^2)|E|^2\ . \tag{1.12}$$

The parameter v in Eqs. (1.10) could be removed by appropriate rescalings but we prefer not to do so for clarity. Equations (1.8)–(1.10) hold inside the electron beam, and can also be used outside the beam if there the right-hand side of Eq. (1.10) is put equal to zero.

Equations (1.8)–(1.10) are well known. In their solution the propagation term $v\,\partial/\partial\eta$ has often been neglected, assuming, e.g., that the slip vL_0 during the interaction time (the time the electrons spend in the undulator of length L_0) is small compared to the pulse length L_b of the electron beam. In a recent paper, Bonifacio and McNeil[3] have given a numerical solution of Eqs. (1.8)–(1.10) including the propagation term. The solution was based on a suitable discretization in space and time. In their solutions the authors of Ref. 3 observed the appearance of a pulse of emitted radiation at the rear end of the pulsed electron beam, and a subsequent strong enhancement of this pulse as it travels through the electron beam with relative velocity vc as seen from the laboratory system. The physical origin of this pulse and the reason for the strong gain it experiences remained unclear.

The present paper is devoted to a more detailed investigation of Eqs. (1.8)–(1.10) including the propagation term. It became clear, during these investigations, that the radiation pulse observed in Ref. 3 is the result of the general sideband instability (cf., e.g., Ref. 4), which appears in the spatially homogeneous saturated state as soon as the propagation term $v\,\partial/\partial\eta$ is taken into account, and which will amplify any spatial inhomogeneity of the combined electron-electromagnetic field system within a certain band of wave numbers. The pulse of Ref. 3 is caused just by the spatial inhomogeneity introduced by the rear end of the electron pulse which is assumed to be sharp in the numerical simulations.

In order to obtain a more realistic prediction for the time dependence and the spectrum of the emitted radiation it seems necessary to take into account other spatial inhomogeneities as well, namely, the random spatial inhomogeneities due to the shot noise in the electron beam. This goal will be achieved here by solving Eqs. (1.8)–(1.10) via a discretization in space but, in contrast to Ref. 3 without discretization in time. This allows us to treat accurately even the tiny fluctuations in the initial conditions due to shot noise. The numerical method is explained in Sec. II. It is applied in Sec. III to the solution of Eqs. (1.8)–(1.10). A qualitative and quantitative understanding of the basic instability is achieved by a combination of a linear stability analysis of a new two-parameter family of spatially homogeneous solutions with further numerical investigations in Secs. IV and V. In Sec. VI we examine the influence of the instability on the emitted spectrum. Our conclusions are summarized in Sec. VII.

II. PETROV GALERKIN DISCRETIZATION

A reliable numerical simulation of Eqs. (1.8)–(1.10) requires a careful choice of their discretization. For clarity we shall discuss the necessary considerations for the simple scalar wave equation

$$\frac{\partial U}{\partial t}=-c\frac{\partial U}{\partial x},\quad t>0\ . \tag{2.1}$$

Let the x axis be discretized with a small step size h, $x_n=nh$. A simple semidiscretization of Eq. (2.1) is obtained via the Galerkin method,[5,6] which yields

$$\frac{1}{6}\left[\frac{dU_{n-1}}{dt}+4\frac{dU_n}{dt}+\frac{dU_{n+1}}{dt}\right]=-c\frac{U_{n+1}-U_{n-1}}{2h}\ , \tag{2.2}$$

with

$$U(x,t)\simeq\sum_n\varphi_n(x)U_n(t)\ ,$$
$$\varphi_n(x)=\begin{cases}1-\left|\dfrac{x-x_n}{h}\right|, & |x-x_n|<h\\ 0\quad\text{otherwise}\ .\end{cases} \tag{2.3}$$

The discretization (2.2) is conservative, i.e., for any square-integrable initial condition

$$\|U(x,0)\|^2\equiv\int dx\ U^2(x,0)<\infty$$

the "energy" $\|U(x,t)\|^2$ is conserved

$$\frac{d}{dt}\|U(x,t)\|^2=0\ . \tag{2.4}$$

Yet this discretization is unsatisfactory, because it generates unphysical oscillations at small wavelengths. For example, there appear oscillations of wavelength $2h$ which travel with negative group velocity, i.e., into a regime of the (t,x) plane totally inaccessible to any solution of the original Eq. (2.1).

A more general semidiscretization of Eq. (2.1) is obtained via the Petrov Galerkin method[7] which yields in place of Eq. (2.2)

$$\frac{1}{6}\left[(1+\tfrac{3}{2}\epsilon)\frac{dU_{n-1}}{dt}+4\frac{dU_n}{dt}+(1-\tfrac{3}{2}\epsilon)\frac{dU_{n+1}}{dt}\right]$$
$$=-\frac{c}{2h}(U_{n+1}-U_{n-1})+\epsilon\frac{c}{2h}(U_{n-1}-2U_n+U_{n+1})\ , \tag{2.5}$$

with a free real parameter ϵ. For $\epsilon=0$ Eq. (2.2) is recovered. The second term on the right-hand side of Eq. (2.5) is seen to introduce some dissipation. For a suitable choice of ϵ it can be used to damp out the unphysical oscillations. Equation (2.5) [like Eq. (2.1)] has plane-wave solutions

$$U_{k,n}(t)=V_k(0)e^{ikx_n}e^{A(k)t}\ , \tag{2.6}$$

with[8]

$$A(k)=-\frac{3c}{h}\frac{i\sin(kh)-\epsilon[\cos(kh)-1]}{2+\cos(kh)-i\frac{3}{2}\epsilon\sin(kh)}$$
$$\simeq-ick-\frac{\epsilon c}{24h}(kh)^4+O((kh)^5)\ . \tag{2.7}$$

Equation (2.6) should be compared with the exact solution of Eq. (2.1)

$$U_k(x,t)=V_k(0)e^{ik(x-ct)} . \tag{2.8}$$

The phase velocity

$$c^*(kh)=-\frac{\mathrm{Im}\,A(k)}{k} \tag{2.9}$$

following from Eq. (2.7) is, for $|kh|\ll 1$,

$$\frac{c^*(kh)}{c}=1-\left[\frac{1}{180}-\frac{\epsilon^2}{48}\right](kh)^4+O((kh)^6) . \tag{2.10}$$

For $\epsilon=2/\sqrt{15}$ one achieves an optimal matching of the phase velocity.

The damping constant

$$\gamma(kh)=-\frac{h}{c}\mathrm{Re}\,A(k) \tag{2.11}$$

for $|kh|\ll 1$ takes the form

$$\gamma(kh)=\frac{\epsilon}{24}(kh)^4+O((kh)^6) , \tag{2.12}$$

while

$$\gamma(kh=\pi)=6\epsilon . \tag{2.13}$$

The dissipation disappears only for $\epsilon=0$. However, even for $\epsilon>0$ it remains very small for $|kh|\ll 1$ and can be used to effectively damp unphysical oscillations at small wavelengths. The group velocity is given by

$$v_G(kh)=-\frac{d}{dk}\mathrm{Im}\,A(k) . \tag{2.14}$$

For large wavelengths $|kh|\ll 1$

$$\frac{v_G(kh)}{c}=-1-\left[\frac{1}{36}-\frac{5\epsilon^2}{48}\right](kh)^4+O((kh)^6) , \tag{2.15}$$

while for small wavelengths, e.g., $kh=\pi$, it is negative, e.g.,

$$v_G(kh=\pi)=-(3+9\epsilon^2)c . \tag{2.16}$$

For $\epsilon>2/\sqrt{15}$ it exceeds c in some range of $kh<\pi$, i.e., ϵ should be restricted to $0<\epsilon<2/\sqrt{15}$. In practice one therefore has to choose ϵ in the range $0<\epsilon<2/\sqrt{15}$ at a value sufficiently large to damp out the unphysical waves with negative group velocities near $kh=\pi$, but sufficiently small in order to keep the dissipation at long wavelengths $|kh|\ll 1$ as small as possible.

A complication arises if Eq. (2.1) is considered on a finite domain $0\le x\le L$. For the cases we shall consider in Sec. III the function U is specified for all times at x_{-1} but it is not specified for $x_{n_{\max}+1}$ where $n_{\max}=L/h$. As $U_{n_{\max}+1}$ is unknown the basis function $\varphi_{n_{\max}+1}$ in Eq. (2.3) must be replaced by 0. As a result the Galerkin and the Petrov Galerkin discretization at $x_{n_{\max}}$ are modified and the latter now reads

$$\frac{1}{6}\left[(1+\tfrac{3}{2}\epsilon)\frac{dU_{n_{\max}-1}}{dt}+(2+\tfrac{3}{2}\epsilon)\frac{dU_{n_{\max}}}{dt}\right]=-\frac{c}{2h}[(1+\epsilon)U_{n_{\max}}-(1+\epsilon)U_{n_{\max}-1}] . \tag{2.17}$$

Even though this discretization is less accurate than the discretization (2.5) in the bulk this causes no problems because the error cannot propagate back into the domain $x<L$ and is therefore guaranteed to remain small.

III. NUMERICAL SIMULATION OF THE NONLINEAR WAVE EQUATIONS

A. Choice of parameters

The wave equations (1.1)–(1.3) contain a natural smallest length scale, the wavelength λ. In the units used in Eqs. (1.8)–(1.10)

$$\lambda_\eta=2k_0\rho\lambda . \tag{3.1}$$

The natural step size for the semidiscretization of the coordinate η/v then is

$$h=\Delta(\eta/v)=\lambda_\eta/v=4\pi\rho[1+O(1/\gamma^2)] . \tag{3.2}$$

In all of our computations we have chosen the value $4\pi\rho=0.3$. The length of the pulse of electrons in the laboratory system is taken as $N_b=200$ optical wavelengths, i.e., the number of steps $\Delta(\eta/v)=h$ in the electron beam is given by N_b. The length of the electron beam in the scaled coordinate η/v then becomes

$$l_b/v=\lambda_\eta N_b/v=60 . \tag{3.3}$$

Note that this parameter is also the scaled time it takes a photon emitted at the rear end of the electron beam to travel to the front end of the beam and leave it there. The scaled time it takes the highly relativistic electrons to pass the undulator of length $L_0=N_0\lambda_0$ once is obtained from Eq. (1.11) as

$$\tau_{\mathrm{int}}=4\pi\rho N_0 . \tag{3.4}$$

The number N_0 of undulator periods is typically between 100 and 200. Thus $\tau_{\mathrm{int}}=30$–60 in the cases we shall consider. The inverse of the parameter (3.3) has been called "superradiance parameter" κ, while the ratio $S=\tau_{\mathrm{int}}/(l_b/v)$ was called slippage parameter. In our case $\kappa\ll 1$ and S is of order 1.

B. Homogeneous initial conditions

The first computations we have carried out neglected shot noise. These runs also served to find an optimal choice for the parameter ϵ of the Petrov Galerkin method. As initial conditions we choose a homogeneous electric field of scaled intensity $|A(\eta,\tau=0)|^2=2\times 10^{-4}$. The number n of electrons within an optical wavelength (realistically $N\approx 10^5$) we choose as $n=50$. We have checked that an increase of n to 100 or 200, while drastically increasing the computation time, had negligible effects on the output. The initial positions of the elec-

trons in these first runs were fixed as $\sigma_j(\eta,\tau=0)=2\pi j/n$ for $j=1,2,\ldots,n$. Therefore $n^{-1}\sum_j e^{i\sigma_j(\eta,\tau=0)}=0$. The initial energy of the electrons was taken as $p_i(\eta,\tau=0)=0$, i.e., shot noise was neglected. As boundary condition at the rear end of the electron beam, $\eta=0$, we assumed $|A(\eta=0,\tau)|^2=2\times10^{-4}$.

In Fig. 1 we plot the intensity $|A|^2$ obtained when taking $\epsilon=0$, i.e., using the Galerkin semidiscretization. It can be seen that the emitted electromagnetic field consists of two components, one component for $\eta/v>\tau$ whose intensity is homogeneous along the electron beam (independent of η) and oscillatory, with variable period, in time τ, and a second component for $\eta/v<\tau$ consisting of pulses emerging from the rear end ($\eta=0$) which are strongly amplified while traveling with group velocity v along the electron beam. However, it can also be seen in Fig. 1 that near the rear end of the electron beam there appear oscillations at very small wavelengths traveling with negative group velocities towards $\eta=0$ and being reflected there. This is an unphysical effect, introduced by the Galerkin discretization as discussed in Sec. II. Therefore the regime $\eta/v<\tau$ is not reliably represented by Fig. 1. In Fig. 2 we show the result corresponding to Fig. 1 but obtained for $\epsilon=0.3$. This value, which was used in all the following computations, was found to give a good compromise between optimal matching of the phase velocity (at $\epsilon=2/\sqrt{15}$) and small dissipation for $|kh|\ll1$. The unphysical small wavelength components with negative group velocities are absent in Fig. 2, which can now be assumed to portray faithfully the emitted radiation intensity. The pulse with positive gain seen in Fig. 2 was discovered by Bonifacio and McNeil[3] in a numerical simulation of Eqs. (1.8)–(1.10) using similar parameter values. These authors speculated that the pulse results from a "superradiant sideband instability" restricted to the domain $\eta/v<\tau$. Indeed, from Fig. 2 it might appear that the instability is somehow connected to the rear end of the electron beam but the reason for this is not at all clear. In order to investigate this question it is necessary to take into account the small spatial inhomogeneities in the initial conditions caused by the shot noise in the electron beam.

C. Initial conditions with shot noise

For N electrons randomly distributed over the optical wavelength λ we have upon averaging over this distribution (denoted by $\langle\ \rangle$)

$$\left\langle\frac{1}{N}\sum_{k=1}^{N}e^{-i\sigma_k}\right\rangle=0\ ,\qquad \left\langle\frac{1}{N^2}\sum_{k,l=1}^{N}e^{i(\sigma_k-\sigma_l)}\right\rangle=\frac{1}{N}\ . \tag{3.5}$$

A realistic value is $N\simeq10^5$. In order to numerically simulate the shot noise (3.5) with $n\ll N$ electrons we place each of the n electrons close to the average position $\langle\sigma_k(\eta)\rangle=2\pi k/n$, $k=1,2,\ldots,n$ according to independent probability distributions with width Δ. If we choose, e.g., normal distributions around these mean values we have

$$\sigma_k(\eta)=\frac{2\pi k}{n}+x_k\ , \tag{3.6}$$

$$P(x_k)=\frac{1}{(2\pi\Delta^2)^{1/2}}\exp\left[-\frac{x_k^2}{2\Delta^2}\right]\ . \tag{3.7}$$

We shall assume $\Delta\ll\pi$ (cf. below) and we can therefore neglect the fact that $P(x_k)$ must be 2π periodic in x_k in order to conform with the fact that the $\sigma_k(\eta)$ are defined in the interval $0\le\sigma_k(\eta)<2\pi$. We can now fix Δ in such a way that

$$\frac{1}{N}=\frac{1}{n^2}\left\langle\sum_{k,l=1}^{n}e^{i(\sigma_k-\sigma_l)}\right\rangle=\frac{1}{n}(1-e^{-\Delta^2})\ . \tag{3.8}$$

For $n\ll N$ we obtain

$$\Delta=\left[\frac{n}{N}\right]^{1/2}\left[1+O\left[\frac{n}{N}\right]\right]\ . \tag{3.9}$$

The same relation is obtained if instead of normal distributions (3.7) we assume equidistributions in a small interval with the same standard deviation. In the example shown in Fig. 3 we choose $N=10^5$, $n=50$ and hence

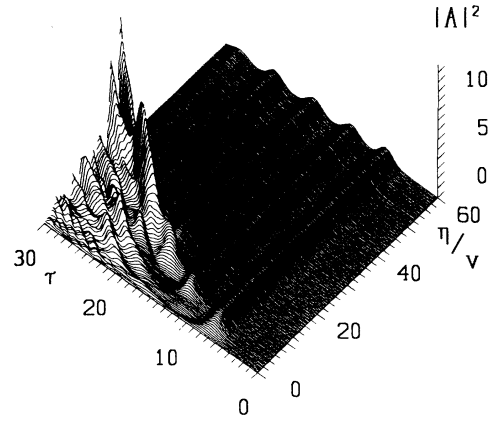

FIG. 1. Intensity $|A(\eta,\tau)|^2$ for $|A(\eta,0)|^2=|A(0,\tau)|^2=2\times10^{-4}$ and $\epsilon=0$.

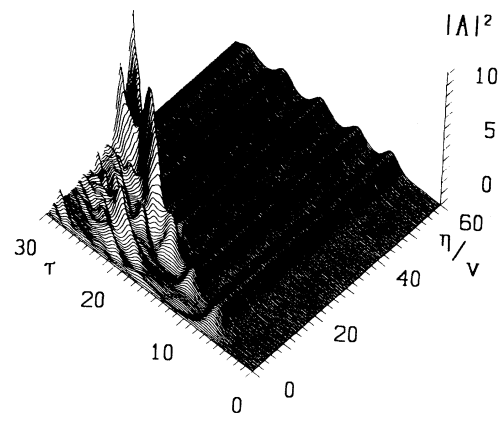

FIG. 2. The same as Fig. 1 for $\epsilon=0.3$.

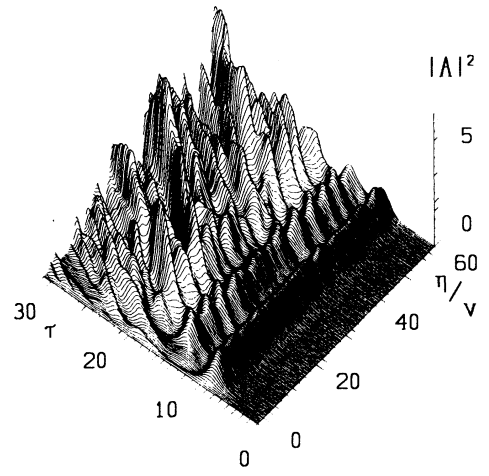

FIG. 3. Intensity $|A(\eta,\tau)|^2$ for $|A(\eta,0)|^2=|A(0,\tau)|^2=2\times10^{-4}$, $\epsilon=0.3$, and shot noise for 10^5 particles per wavelength.

$\Delta=2.2\times10^{-2}$. Otherwise we assume the same initial conditions as in Fig. 2. We show the result for the scaled field intensity obtained under these conditions. It is now obvious that the pulses develop not only from the rear end of the electron beam but everywhere, starting from shot noise. The special role of the rear end in Fig. 2 is simply caused by the (unrealistic) fact that there the end of the pulse is the only spatial inhomogeneity present in the initial condition.

The questions remain, what is the nature of the instability shown in Fig. 3, and what determines the length scale and the amplification rate of the pulses of radiation found there. These questions are dealt with next.

IV. INSTABILITY DUE TO PROPAGATION EFFECTS

If propagation effects are neglected the emitted radiation intensity is constant over the electron beam and oscillates in time nearly harmonically. We shall first construct a two-parameter family of spatially homogeneous analytic solutions describing this behavior and then apply a linear stability analysis to investigate the influence of spatially inhomogeneous small fluctuations.

A. Spatially homogeneous solution

Assuming all fields to be independent of η Eqs. (1.8)–(1.10) become

$$\frac{d^2\sigma_j}{d\tau^2}=-\frac{\partial}{\partial\sigma_j}V_p(\sigma_j)\ ,\qquad \frac{dA(\tau)}{d\tau}=\frac{1}{N}\sum_j e^{-i\sigma_j(\tau)}\ , \tag{4.1}$$

where the ponderomotive potential $V_p(\sigma)$ is given by

$$V_p(\sigma)=2a(\tau)\sin[\sigma(\tau)+\varphi(\tau)]\ , \tag{4.2}$$

with

$$A(\tau)=a(\tau)e^{i\varphi(\tau)},\quad a>0\ . \tag{4.3}$$

Equations (4.1) imply two conservation laws

$$\frac{1}{N}\sum_j\dot\sigma_j+|A|^2=c_1\ ,\qquad \frac{1}{N}\sum_j[\tfrac{1}{2}\dot\sigma_j^2+i(A^*e^{-i\sigma_j}-Ae^{i\sigma_j})]=c_2\ , \tag{4.4}$$

where c_1,c_2 are two real constants determined by the initial condition.

A time-independent solution for $a(\tau)$ is possible if all electrons sit in the minimum of the ponderomotive potential, i.e., if

$$\sigma_j(\tau)=\frac{3\pi}{2}-\varphi(\tau)\ ,\qquad \frac{1}{N}\sum_j e^{-i\sigma_j(\tau)}=ie^{i\varphi(t)}\ . \tag{4.5}$$

From Eq. (4.1) we then obtain

$$\varphi(\tau)=\nu\tau\ ,\qquad a\nu=1\ . \tag{4.6}$$

Physically, this solution describes the free-electron laser in saturation, where no further exchange of energy between the electrons and the radiation field is possible. A similar one-parameter family of solutions was obtained in Ref. 4, but there the phase φ was assumed to be independent of τ and to vary linearly in η, instead. The electron energy

$$\gamma_j=\gamma_r(1-\rho\nu)<\gamma_r \tag{4.7}$$

is below the resonance energy, and the scaled field intensity is constant

$$|A|^2=1/\nu^2\ . \tag{4.8}$$

As there is only one free parameter ν these solutions are only possible for special initial conditions satisfying

$$c_1=-\nu+\frac{1}{\nu^2},\quad c_2=-\frac{2}{\nu}+\frac{\nu^2}{2}\ . \tag{4.9}$$

However, we shall now generalize the solution and obtain a new two-parameter family, which allows us to accommodate more general initial conditions. Let us assume for this purpose that the phases of the electrons are distributed with some density P_σ around the value (4.5), i.e.,

$$\sigma_j=\frac{3\pi}{2}-\nu\tau+x_j\ , \tag{4.10}$$

where $-\pi<x_j\le\pi$ and

$$P_\sigma(x)=\frac{1}{2\pi}\sum_{k=-\infty}^{\infty}e^{ikx-(1/2)\Delta_\sigma^2k^2}\ . \tag{4.11}$$

Then $\langle x_j\rangle=0$ and

$$\langle x_j^2\rangle=\frac{\pi^2}{3}+4\sum_{k=1}^{\infty}\frac{(-1)^k}{k^2}e^{-(1/2)\Delta_\sigma^2k^2}\ . \tag{4.12}$$

In the following we restrict ourselves to $\Delta_\sigma\le1$ and may then approximate $\langle x_j^2\rangle^{1/2}\simeq\Delta_\sigma$ and

$$P_\sigma(x)\simeq\frac{1}{(2\pi\Delta_\sigma^2)^{1/2}}\exp\left[-\frac{x^2}{2\Delta_\sigma^2}\right], \tag{4.13}$$

where now $-\infty<x<+\infty$. In the solution we wish to construct here the width Δ_σ shall remain constant. This can be achieved by assuming the "momenta" $p_j=\dot{\sigma}_j$ to be suitably distributed with some density P_p

$$p_j=-\nu+y_j\ , \tag{4.14}$$

where $-\infty<y_j<+\infty$. We try again a normal distribution

$$P_p(y)=\frac{1}{(2\pi\Delta_p^2)^{1/2}}\exp\left[-\frac{y^2}{2\Delta_p^2}\right]. \tag{4.15}$$

For the field we again make the ansatz (4.3). Inserting Eqs. (4.10) and (4.3) in Eq. (4.1) we obtain

$$\ddot{x}_j+2a\sin x_j=0\ . \tag{4.16}$$

For $|x_j|$ sufficiently small ($|x_j|<1$) the solution reads

$$\begin{aligned}x_j&=x_{0j}\cos\omega\tau+y_{0j}\sin\omega\tau\ ,\\ y_j&=-x_{0j}\omega\sin\omega\tau+y_{0j}\omega\cos\omega\tau\ ,\end{aligned} \tag{4.17}$$

with

$$\omega^2=2a\left[1-\frac{x_{0j}^2+y_{0j}^2}{8}\right]\simeq 2a\ . \tag{4.18}$$

Here x_{0j} and y_{0j} are independent random numbers with vanishing average. The condition $\Delta_\sigma=$const implies $\langle x_j^2\rangle=$const, which is satisfied if we choose

$$\langle x_{0j}^2\rangle=\langle y_{0j}^2\rangle\ . \tag{4.19}$$

Hence

$$\Delta_p^2=\langle y_j^2\rangle=\langle\omega^2x_j^2\rangle\simeq 2a\Delta_\sigma^2\ , \tag{4.20}$$

where Δ_σ^2 should be sufficiently small ($\Delta_\sigma^2<1$) to validate our approximations. Within this restriction we now have the two-parameter family of spatially homogeneous solutions

$$\begin{aligned}A&=ae^{i\nu\tau}\ ,\\ \sigma_j&=\frac{3\pi}{2}-\nu\tau+x_j,\quad p_j=-\nu+y_j\ ,\\ P_\sigma(x_j)&\simeq\frac{1}{(2\pi\Delta_\sigma^2)^{1/2}}e^{-x^2/2\Delta_\sigma^2}\ ,\\ P_p(y_j)&\simeq\frac{1}{(4\pi a\Delta_\sigma^2)^{1/2}}e^{-y^2/4a\Delta_\sigma^2}\ .\end{aligned} \tag{4.21}$$

From Eq. (4.1) follows the condition

$$a\nu=e^{-(1/2)\Delta_\sigma^2} \tag{4.22}$$

replacing Eq. (4.6).

The conservation laws (4.4) now permit one to determine the two free parameters a and ν from the initial conditions. Assuming that initially all the electrons have the resonance energy $\gamma_j=\gamma_r$, i.e., $p_i=0$, and $A\simeq 0$ we may take $c_1=0=c_2$. Evaluating now the left-hand sides of Eqs. (4.4) for our two-parameter family we obtain with $b=\exp(-\frac{1}{2}\Delta_\sigma^2)$

$$b=\exp(-3b/4) \tag{4.23}$$

and hence

$$a=b^{1/3}\simeq 0.86,\quad \nu=b^{2/3}\simeq 0.73\ . \tag{4.24}$$

If instead, the electrons are not monoenergetic, initially, but are symmetrically distributed around the resonance energy with width $\langle p^2\rangle_0^{1/2}$, we have instead $c_2=\frac{1}{2}\langle p^2\rangle_0$ and Eq. (4.23) is replaced by $b=\exp[-3b/4-c_2/(2b^{1/3})]$. The numerical values in Eqs. (4.24) are reduced, accordingly. In view of the nearly harmonic oscillations of the spatially homogeneous solution visible in Figs. 1 and 2 it is instructive to extend our two-parameter family of solutions even further by allowing small oscillations. The necessary analysis is a linearization around the solution (4.21). This linearized analysis will be extended to the spatially inhomogeneous case in the next section. With the ansatz

$$\begin{aligned}A&=[a+\alpha(\tau)]e^{i\nu\tau}\ ,\\ \langle\sigma\rangle&=\frac{3\pi}{2}-\nu\tau+\langle\delta\sigma(\tau)\rangle\ ,\end{aligned} \tag{4.25}$$

and introducing the variables

$$\begin{aligned}R&=\alpha+\alpha^*\ ,\\ I&=i(\alpha+\alpha^*)\ ,\\ S&=\langle\delta\sigma\rangle\ ,\end{aligned} \tag{4.26}$$

we obtain, after linearization, the following system:

$$\begin{aligned}&\left[2ab+\frac{d^2}{d\tau^2}\right]S-bI=0\ ,\\ &-2bS+\frac{d}{d\tau}R+\frac{b}{a}I=0\ ,\\ &-\frac{b}{a}R+\frac{d}{d\tau}I=0\ .\end{aligned} \tag{4.27}$$

The two eigenvectors with vanishing eigenvalues are of no interest because they only describe the freedoms of our two-parameter family, which we have already fixed by the initial conditions. Hence there remains

$$\begin{aligned}\langle\sigma_j\rangle&=\frac{3\pi}{2}-\nu\tau+\beta\sin(\omega\tau+\varphi)\ ,\\ A&=a\left[1-\frac{\beta\omega}{2a^2}\cos(\omega\tau+\varphi)\right]\\ &\quad\times\exp\left[i\left[\nu\tau+\frac{\beta\nu}{2a^2}\sin(\omega\tau+\varphi)\right]\right]\ ,\end{aligned} \tag{4.28}$$

where

$$\frac{\beta\omega}{2a^2}\ll 1 \tag{4.29}$$

and

$$\omega=\nu\left[1+\frac{2a^2}{\nu}\right]^{1/2} . \tag{4.30}$$

From Eqs. (4.24) we obtain

$$\omega=\sqrt{3}\nu\simeq 1.27 . \tag{4.31}$$

We have checked these results by solving the spatially homogeneous equations for 400 electrons and analyzing $|A(\tau)|$; its Fourier transform

$$|\tilde{A}(\omega)|=\left|1/T\int_0^T d\tau e^{i\omega\tau}|A(\tau)|\right| ,$$

and the phase $\varphi(\tau)$ are shown in Fig. 4, which shows that $|A(\tau)|$ essentially consists of a constant $a\simeq 0.76$ and an oscillatory part with frequency $\omega\simeq 1.28$ and that the phase $\varphi(\tau)$ increases linearly, on the average with $\nu\simeq 0.71$. From the good agreement of these results with the analytical solution we conclude that the spatially homogeneous solution is now well understood and turn to spatially inhomogeneous perturbations.

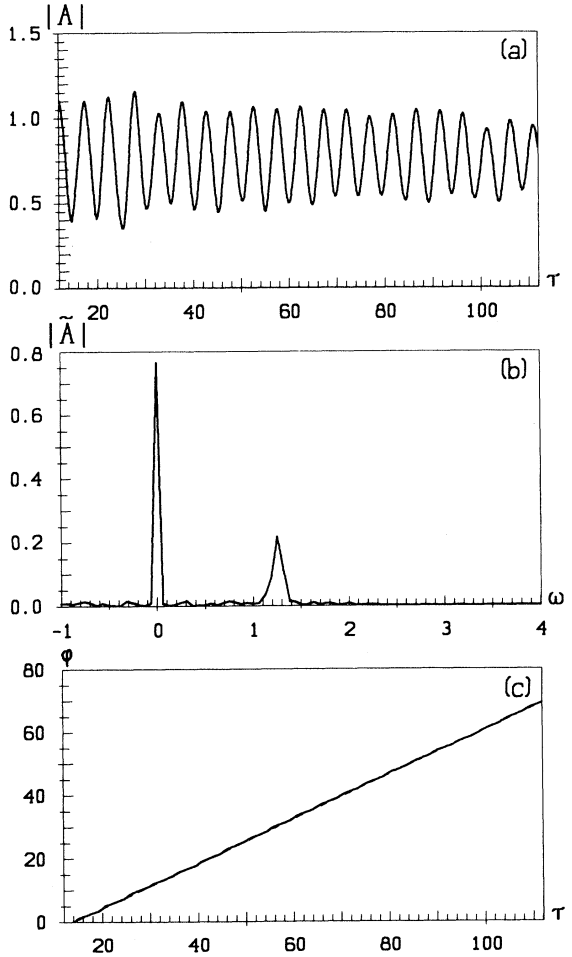

FIG. 4. (a) Absolute value of spatially homogeneous solution $|A(\tau)|$, (b) Fourier transform of $|A(\tau)|$, and (c) phase of $A(\tau)$.

B. Linear analysis of spatially inhomogeneous fluctuations

The ansatz (4.27) with $\alpha, \langle\delta\sigma\rangle$ small and proportional to $\exp(ik\eta/v-i\omega\tau)$, after linearization, yields Eq. (4.27), with the replacements $d^2/d\tau^2\to-\omega^2$, $d/d\tau\to-i(\omega-k)$. We obtain the dispersion relation

$$D(k,\omega)=(2ab-\omega^2)\left[\left[\frac{b}{a}\right]^2-(\omega-k)^2\right]-\frac{2b^3}{a}=0 . \tag{4.32}$$

We shall assume k to be given as real. A similar dispersion relation holds for the one-parameter family (4.5) and (4.6).[4] An instability shows up by the appearance of complex-conjugate pairs of solutions for ω. For $k=0$ one finds $\omega_{1,2}=0$, $\omega_{3,4}=\pm\nu(1+2a^2/\nu)^{1/2}$, the result given in Eqs. (4.27). An instability exists for all k in the interval $0<|k|<k_{\max}$ where $k_{\max}$ is obtained as

$$k_{\max}=\frac{b^{1/2}}{a}(b^{1/3}+2^{1/3}a)^{3/2}$$
$$=\nu\left[1+\left[\frac{2a^2}{\nu}\right]^{1/3}\right]^{3/2} . \tag{4.33}$$

This result tells us that, in order to suppress the instability visible in Fig. 2, the scaled pulse length L_b of the electron beam must be shorter than

$$\frac{L_b}{v}<\frac{2\pi}{k_{\max}} , \tag{4.34}$$

i.e., in unscaled units

$$l_b<l_c=\frac{\beta_\parallel\lambda}{2\rho k_{\max}} . \tag{4.35}$$

For a laser initiated by shot noise we find with $\beta_\parallel\simeq 1$ and the calculated values $a\simeq 0.86$, $\nu\simeq 0.73$

$$k_{\max}\simeq 2.5, \quad l_c\simeq\frac{\lambda}{5\rho} . \tag{4.36}$$

The quartic dispersion relation is most easily evaluated for $|k|\ll 1$ and for $|k|\gg 1$. In the special case $2a^3=b$ (i.e., $\nu=2a^2$) the quartic reduces to a biquadratic equation and we obtain

$$\omega(k)=\frac{k}{2}\pm((k/2)^2+\nu^2\{1\pm[1+(k/\nu)^2]^{1/2}\})^{1/2} \tag{4.37}$$

and $k_{\max}=2^{2/3}\nu$.

The typical k dependence of the roots of the dispersion relation $\omega(k)$ is shown in Fig. 5, obtained numerically for $a=0.86$, $b=0.63$. The unstable window $0<|k|<k_{\max}$ with $\mathrm{Im}\omega(k_0)\neq 0$ is clearly visible. There is a wave number k_0 where $|\mathrm{Im}\omega(k_0)|$ is maximal. In the special case $2a^3=b$ we have $k_0=\sqrt{3}\nu$, $\omega(|k_0|)=(\sqrt{3}/2)\nu\pm i(\nu/2)$. In Fig. 6 we plot $|\mathrm{Im}\omega(k_0)|$ as a function of a for the two fixed values $b=1$, $b=0.63$. We also show as dashed lines two asymptotic analytic results

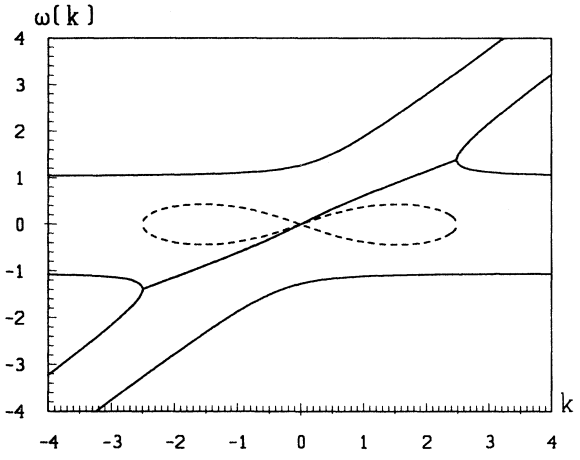

FIG. 5. Real part (solid line) and imaginary part (dashed line) of $\omega(k)$ for $a=0.86$ and $b=0.63$.

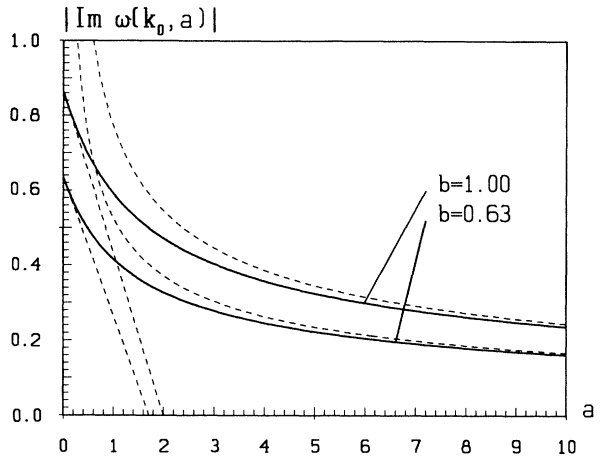

FIG. 6. Maximal growth rate $|\mathrm{Im}\omega(k_0)|$ as a function of a, and asymptotic results (dashed line) for $a \ll 1$ and $a \gg 1$.

$$|\mathrm{Im}\omega(k_0)|=\frac{\sqrt{3}}{2}\left[b^{2/3}-\frac{ab^{1/3}}{2}+O(a^2)\right], \quad a\ll 1$$
$$|\mathrm{Im}\omega(k_0)|=\frac{\sqrt{3}}{2}\frac{b}{(2ba^3)^{1/6}}+O\left[\frac{1}{a^{3/2}}\right], \quad a\gg 1 \tag{4.38}$$

obtained from the dispersion relation (4.32). It can be seen in Fig. 6 that these results give analytic lower and upper bounds, respectively, for the maximal linear amplification rate of the instability. An absolute upper bound $|\mathrm{Im}\omega(k_0)|\le\sqrt{3}/2$ is obtained for $b=1$, $a=0$. The main feature seen in Fig. 6 is the increase of the amplification rate with decreasing a, which is plausible because the depth of the binding well of the ponderomotive potential decreases with a, which should favor the instability.

Let us now compare this analysis with the numerical results. We start from a spatially homogeneous solution with $a=0.76$, $\nu=1.15$, $\Delta_\sigma=0.51$ correspondings to $b=0.87$. In this case $2a^2\simeq\nu$ and we can use the dispersion relation (4.37). For $\tau=0$ we perturb the homogeneous solution by a small localized spatial inhomogeneity. In Fig. 7 the radiation pulse $|A|^2$ with $A=A_h(\tau)+A_s(\eta,\tau)$ is shown, where $A_h(\tau)$ is the unperturbed spatially homogeneous field. For $\tau>15$ the perturbation is no longer small, and the linear analysis cannot be expected to apply. In Figs. 8(a)–8(d) the real and imaginary part of A_s are shown together with their spatial spectrum for the times $\tau=0,6,15,21$, respectively. At $\tau=15$ the spectrum has shrunk to wave numbers $|k|<3.2$ in good agreement with $k_{\max}=2^{3/2}\nu\simeq 3.3$. The maximally amplified wave number is predicted as $|k_0|=(\sqrt{3}/2)\nu\simeq 2.0$ in excellent agreement with the spectrum at $\tau=15$ which peaks at sidebands $k\simeq\pm 2$. In the nonlinear domain higher-order sidebands near $k\simeq\pm 4$ and $k\simeq 6$ are seen to appear. The exponential increase of the amplitude of the maximally amplified perturbation $|\tilde{A}_s(k_0)|$ is shown in a semilogarithmic plot in Fig. 9.

The extracted amplification rate $|\mathrm{Im}\omega(k_0)|=0.56$ agrees well with the predicted value $|\mathrm{Im}\omega(k_0)|=\nu/2\simeq 0.57$, in particular if taking into account that the Petrov Galerkin discretization introduces a damping rate $\gamma(|k|=2,h=0.3)/h\simeq 6\times 10^{-3}$ which slightly decreases the numerical amplification rate.

V. EMITTED SPECTRUM

We now calculate the power spectrum emitted in the nonlinear regime. The spectrum emitted in the initial regime of linear amplification has been calculated in a preceding paper.[9]

Our aim is to determine the spectrum which can be observed at a position $z=\tilde{z}/2k_0\rho$ fixed in the laboratory over a finite time interval $\tilde{z}-L_b<\tau<(\tilde{z}-L_b)/(1-v)$. It is defined as

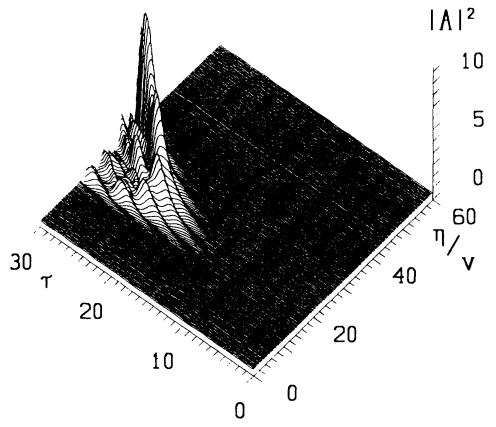

FIG. 7. Radiation pulse caused by a local perturbation of the spatially homogeneous solution with $a=0.76$, $\Delta_\sigma=0.51$.

$$P_T(\tilde{z},\tau,\omega)=\frac{1}{T}\langle A_T^*(\tilde{z},\tau,\omega)A_T(\tilde{z},\tau,\omega)\rangle \ , \tag{5.1}$$

with

$$A_T=\int_{-T/2}^{T/2} d\tau' e^{i\omega\tau'} A_>(\tilde{z},\tau+\tau') \ , \tag{5.2}$$

where

$$A_>(\tilde{z},\tau)=A\left[L_b,\frac{\tau+L_b-\tilde{z}}{v}\right] \tag{5.3}$$

is the field in front of the electron beam. For simplicity we choose $\tau=2(\tilde{z}-L)(1+\beta_\parallel)$ in the middle of the time interval $[\tilde{z}-L_b,(\tilde{z}-L_b)/(1-v)]$ and $T=v\tau$, i.e., we assume that the entire available time interval is used for taking the spectrum. Then with $\tilde{z}=L+(1+\beta_\parallel)\tau/2$

$$P_{v\tau}(\tilde{z},\tau,\omega)=\frac{v}{\tau}\int_0^\tau d\tau' \int_0^\tau d\tau'' e^{iv\omega(\tau'-\tau'')} \times\langle A^*(L_b,\tau'')A(L_b,\tau')\rangle \ . \tag{5.4}$$

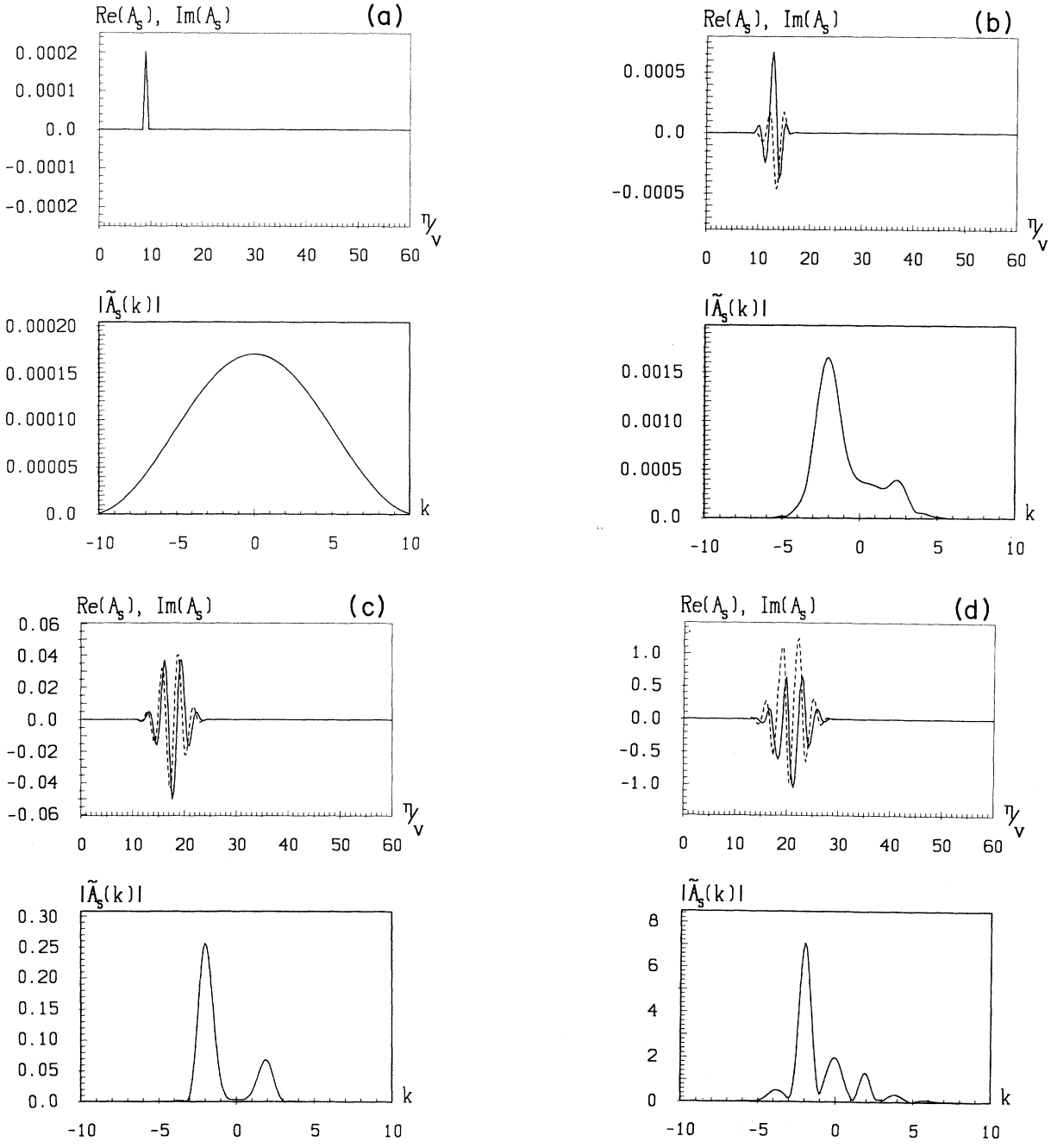

FIG. 8. Real and imaginary parts of A_s and their spatial Fourier transforms for (a) $\tau=0$; (b) $\tau=6$; (c) $\tau=15$; (d) $\tau=21$.

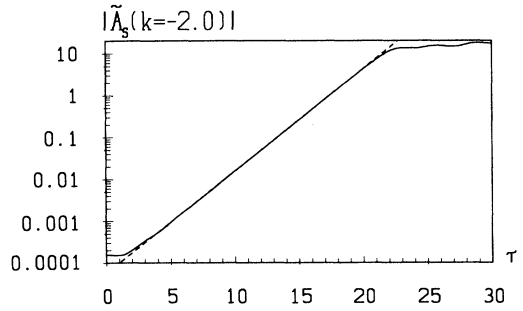

FIG. 9. Amplitude of maximally amplified Fourier mode for $k_0=-2$.

We now use

$$A(L_b,\tau)=[a+\alpha(L_b,\tau)]e^{i\nu\tau}\ , \tag{5.5}$$

where

$$\alpha(L_b,\tau)=\sum_{j=1}^{4}\int dk[R_j(k)-iI_j(k)]\ . \tag{5.6}$$

Here R_j-iI_j $(j=1,\ldots,4)$ are the complex eigenvectors of the linear stability analysis of Sec. IV B, which are easily evaluated as

$$\begin{bmatrix}R_j(k)\\ I_j(k)\end{bmatrix}=c_j(k)\begin{bmatrix}-i[\omega_j(k)-k]\\ \nu\end{bmatrix}\times\exp\left[-i\left[\omega_j(k)\tau-\frac{kL_b}{v}\right]\right]\ . \tag{5.7}$$

We neglect all eigenvectors not growing exponentially in time and therefore drop the index j. We assume the perturbation is caused by shot noise and spatially homogeneous

$$\begin{aligned}&\langle c(k)\rangle=0\ ,\\ &\langle c(k)c^*(k')\rangle=f(k)\delta(k-k')\ ,\end{aligned} \tag{5.8}$$

where $f(k)$ is determined by the particular perturbation. Hence

$$\frac{1}{v}P_{v\tau}\left[\tilde{z},\tau,\frac{\omega}{\tau}\right]=\frac{2a^2}{\tau}\frac{1-\cos[(\nu+\omega)\tau]}{(\nu+\omega)^2}+\frac{1}{\tau}\int_0^\infty dk\,f(k)\left[\left|\frac{\omega(k)-k+\nu}{\omega(k)-\omega-\nu}\right|^2|e^{i[\nu+\omega-\omega(k)]\tau}-1|^2+\left|\frac{\omega(k)-k-\nu}{\omega^*(k)+\omega+\nu}\right|^2|e^{i[\nu+\omega+\omega^*(k)]\tau}-1|^2\right]\ . \tag{5.9}$$

The first term is the spectrum of the spatially homogeneous part and approaches for τ large $2\pi a^2\delta(\omega+\nu)$. The integral is the spectrum of the perturbation. It can be simplified for times τ large compared to the inverse amplification rate (but still sufficiently small to validate the linearization of Sec. IV B). Then the exponentials in the integrand of (5.9) are large compared to 1 and the latter can be dropped. Furthermore the k integral can be done in saddle-point approximation at the saddle point $\mathrm{Im}[d\omega(k)/dk]=0$. We obtain for the spectrum of the perturbation P_p two Lorentzians

$$\frac{1}{v}P_p\left[\frac{\omega}{v}\right]=\frac{f(k_0)}{\tau^{3/2}}e^{2|\mathrm{Im}\omega(k_0)|\tau}\left[\frac{\gamma_-^2}{[\mathrm{Re}\omega(k_0)+\omega+\nu]^2+[\mathrm{Im}\omega(k_0)]^2}+\frac{\gamma_+^2}{[\mathrm{Re}\omega(k_0)-\omega-\nu]^2+[\mathrm{Im}\omega(k_0)]^2}\right]\ , \tag{5.10}$$

with

$$\gamma_\pm^2=[\mathrm{Re}\omega(k_0)-k_0\pm\nu]^2+[\mathrm{Im}\omega(k_0)]^2\ . \tag{5.11}$$

We note that $\mathrm{Re}\omega(0)=0$ and $d\,\mathrm{Re}\omega(k)/dk\le 1$ because the group velocity is smaller than the velocity of light. Therefore $\mathrm{Re}\omega(k_0)\le k_0$ and $\gamma_-^2>\gamma_+^2$. We conclude that the Lorentzian centered at $\omega=-[\nu+\mathrm{Re}\omega(k_0)]$ is always stronger by a factor $(\gamma_-/\gamma_+)^2$ than the Lorentzian around $\omega=-[\nu-\mathrm{Re}\omega(k_0)]$. In other words, the instability shifts some of the electrons trapped by the ponderomotive potential at frequency $\omega=-\nu$ and having relative energy $\langle p\rangle=-\nu$ to new minima of the potential at frequencies $\omega=-[\nu\pm\mathrm{Re}\omega(k_0)]$. The relative energy of these shifted electrons is $\langle p\rangle=-[\nu\pm\mathrm{Re}\omega(k_0)]$. On the average more electrons are shifted to the smaller frequency, because $\gamma_-^2>\gamma_+^2$. Therefore the electrons lose energy on the average, i.e., the radiation field experiences gain in these sidebands which deepens the new potential minima and enhances the transfer of electrons to the sidebands. The ratio $(\gamma_-/\gamma_+)^2$ can also be seen in the spatial spectrum

$$\tilde{A}_s(k,\tau)=\int d\eta\,e^{-ik\eta}\alpha(\eta,\tau)\ . \tag{5.12}$$

We obtain

$$|\tilde{A}_s(k,\tau)|=|c(k)|\,|\omega(k)-k+\nu|e^{\mathrm{Im}\omega(k)\tau} \tag{5.13}$$

and

$$\frac{|\tilde{A}_s(-k_0,\tau)|}{|\tilde{A}_s(k_0,\tau)|}=\frac{\gamma_-}{\gamma_+}\ , \tag{5.14}$$

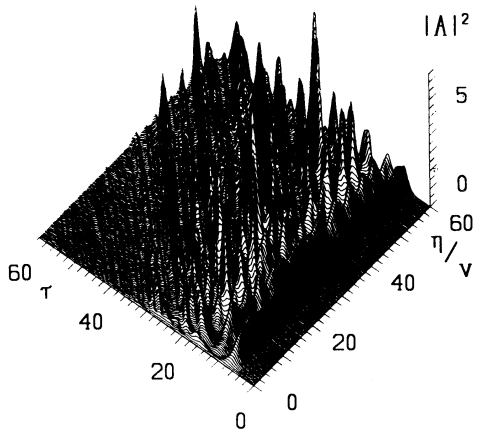

FIG. 10. Intensity $|A(\eta,\tau)|^2$ for larger interaction times τ (long undulators) for the case of Fig. 3.

In the special case $2a^2=\nu$ considered in Fig. 7 we have $\mathrm{Re}\omega(k_0)=(\sqrt{3}/2)\nu$, $\mathrm{Im}\omega(k_0)=\nu/2$, $k_0=\sqrt{3}\nu$, and $\gamma_-/\gamma_+=2+\sqrt{3}\simeq 3.7$ in excellent agreement with the ratio of 3.7 of the two maxima in Fig. 8(c).

Finally we compute the spectrum for longer scaled time starting from a very small initial field ($|A|^2=2\times10^{-4}$) and shot noise. Figure 10 shows the breakup of the initially nearly homogeneous solution into sharp pulses. For $\tau>30$ the group velocity of these pulses has approached the velocity of light and their intensity remains nearly constant.

We compute the spectrum of the radiation field in front of the electron beam at different scaled times τ. The result plotted in Figs. 11(a)–11(c) shows at $\tau=15$ [Fig. 11(a)] a resolution limited peak at $\omega\simeq-0.7$, which is at the expected frequency ν of the spatially homogeneous solution ($\nu\simeq0.73$ from the analytical and $\nu\simeq0.71$ from the numerical homogeneous solution). At $\tau=20$ [Fig. 11(b)] the sideband at frequency $\omega=-[\nu+\mathrm{Re}\omega(k_0)]\simeq-1.6$ is nearly visible. At still later time $\tau=40$ [Fig. 11(c)] many more sidebands at negative frequencies have developed, i.e., the mechanism of the first sideband instability is repeated.

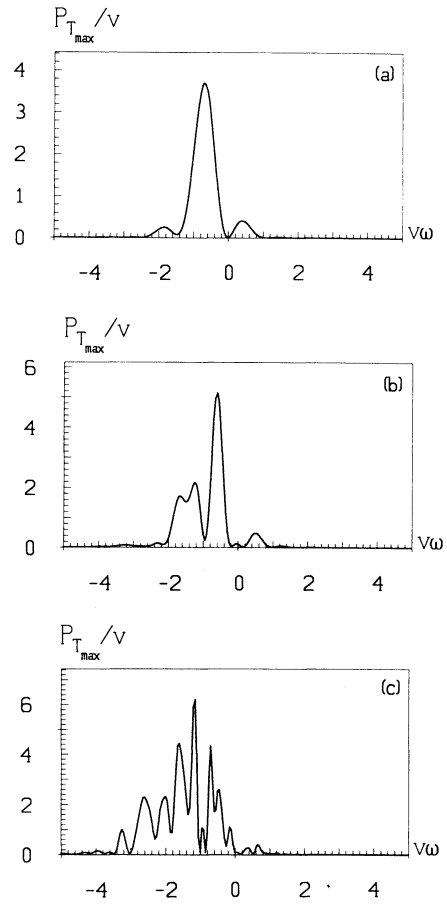

FIG. 11. Spectrum of the emitted radiation for (a) $\tau=15$; (b) $\tau=20$; (c) $\tau=40$.

VI. CONCLUSIONS

The nonlinear coupled wave equations of a free-electron laser in the Compton regime have been studied numerically and analytically for initial conditions which include shot noise. The numerical analysis was based on a systematic semidiscretization scheme, described in Sec. II. Our simulations show that shot noise of a realistic size prohibits the development of the strong radiation pulse at the rear end of the electron beam found by Bonifacio and McNeil[3] and confirmed here for initial conditions neglecting shot noise. Rather, the simulations presented here show that instead pulses of smaller intensity will appear from shot noise throughout the electron beam.

The underlying sideband instability has been exhibited analytically for a two-parameter family of spatially homogeneous solutions by performing a linearized analysis of small spatially inhomogeneous perturbations, extending similar earlier work in Ref. 4. A critical length $l_c=\beta_\parallel\lambda/2\rho k_{\max}$ of the pulsed electron beam was found which must not be exceeded if the instability is to be suppressed. However, even in electron beams exceeding the length l_c this parameter is important. It plays the role of a cooperation length of the electrons, because l_c defines the maximum distance over which electrons in the beam can emit cooperatively. The radiation emitted by two electrons at larger distances will end up contributing to two different pulses of radiation. All results of the analysis were compared with detailed simulations and we obtained very good agreement. The sidebands caused by the instability can also be seen in the emitted wave number and frequency spectrum. Further sidebands appear for longer interaction times and can be understood by a repetition of the first instability.

[1]C. Pellegrini, in *Proceedings of the Seventh Course on Physics and Technology of Free Electron Lasers of the International School of Quantum Electronics, Erice, Italy, 1980,* edited by S. Martelucci and A. N. Chester (Plenum, New York, 1983), p. 91.

[2]W. B. Colson, in *Proceedings of the Seventh Course on Physics and Technology of Free Electron Lasers of the International School of Quantum Electronics, Erice, Italy, 1980,* edited by S. Martelucci and A. N. Chester (Plenum, New York, 1980), p. 189.

[3]R. Bonifacio and B. W. J. McNeil, Nucl. Instrum. Methods A **272,** 20 (1988).

[4]R. C. Davidson and J. S. Wurtele, Phys. Fluids **30,** 557 (1987).

[5]K. W. Morton and A. K. Parrot: Comput. Phys. **36,** 249 (1980).

[6]K. W. Morton, Comput. Methods Appl. Mech. Eng. **52,** 847 (1985).

[7]D. F. Griffiths, in *The Mathematics of Finite Elements and Applications IV—MAFLEAP 1981,* edited by J. R. Whitman (Academic, London, 1982).

[8]R. Vichnevetsky and J. B. Bowles, *Fourier Analysis of Numerical Approximations of Hyperbolic Equations* (SIAM, Philadelphia, 1982).

[9]R. Graham and S. Isermann, Z. Phys. B **75,** 547 (1989).